View metadata, citation and similar papers at core.ac.uk
brought to you by CORE
provided by RERO DOC Digital Library

Geophys. J. Int. (2008) **173,** 781–792 doi: 10.1111/j.1365-246X.2008.03762.x

Can a 1-D mantle electrical conductivity model generate magnetic jerk differential time delays?

K. Pinheiro and A. Jackson

Institute of Geophysics, ETH Zurich, 8093, Zurich, Switzerland. E-mail: katia@erdw.ethz.ch

Accepted 2008 February 14. Received 2007 December 17

SUMMARY

Worldwide jerks occurring in 1969, 1978 and 1991 are not simultaneous at the earth's surface, showing differential delays of about 2 yr. One way to explain this intriguing temporal pattern is to consider the earth's mantle as a conductor. Consequently the geomagnetic field observed at the earth's surface will correspond to a filtered version of the original field generated at the core–mantle boundary (CMB). We developed the forward approach to this problem assuming the temporal part of the jerk as a simultaneous impulse in the third time-derivative of the magnetic field at the CMB. Two synthetic spherical harmonic models of the jerk amplitudes are built by using two different power spectra. The effect of the mantle is illustrated by a 1-D radial electrical conductivity model that acts as linear, causal and time-invariant filter. The key point is that the mantle filter is different for each harmonic degree. Therefore, because the mixing of harmonics varies with location, distinct time delays will exist at the earth's surface. By using Backus' mantle filter theory, we demonstrate that a simple 1-D mantle electrical conductivity model is able to generate differential jerk time delays that depend strongly on the jerk morphology input model. We also illustrate that the time delays will vary for each component of the magnetic field.

Key words: Geomagnetic induction; Rapid time variations.

1 INTRODUCTION

Most of the geomagnetic field observed at the earth's surface is generated in the core, and its first time-derivative is called secular variation. Geomagnetic jerks are abrupt changes in the trend of the secular variation that can be seen in magnetic observatory data, especially in the *Y* component that is less contaminated by magnetospheric fields (Fig. 1).

Jerks have a typical 'V' shape and can be approximated as straight line segments dividing intervals of linear secular variation. In this simplistic model, jerks can be seen in the second time differences as a step function and in the third differences as an impulse (Fig. 2). Their amplitudes are evaluated by the difference between the slope of consecutive straight lines segments of the secular variation.

The detection and characterization of geomagnetic jerks have been the topic of much debate in the last few decades. The main features under discussion are their local or worldwide extent, their morphologies (i.e. the spatial distribution of amplitude) and whether a same jerk is observed simultaneously at the earth's surface or not. The most well known and studied jerk occurred in 1969 and shows a global behaviour (Malin & Hodder 1982). Other jerks happened in 1901 and 1913 with possible worldwide distributions whereas local jerks occurred first in 1932, mostly observed in the Southern Hemisphere and second in 1949, mainly in the Pacific and American regions (Alexandrescu *et al.* 1996). Worldwide jerks also happened in 1978 and 1991 (Macmillan 1996; De Michelis *et al.* 1998, 2000) and another jerk in 1999 (Mandea *et al.* 2000) was detected in European observatories.

Most jerk studies use monthly or annual means of geomagnetic elements recorded at observatories. The uneven distribution of observatories is a clear limitation for the global analysis of geomagnetic jerks. The use of satellite data overcomes this problem by providing a good spatial coverage of magnetic measurements. Sabaka *et al.* (2004) derived a comprehensive model (CM4) of the geomagnetic field, for the epoch from 1960 to mid-2002, by using hourly means from magnetic observatories and data from satellites (POGO, Magsat, Oersted and CHAMP). This model was able to detect the well-known jerks but found their occurrence times to be 1969, 1979, 1992, 2000 and another jerk of questionable global extent in 1997. Chambodut *et al.* (2007) used synthetic time-series from the CM4 model and localised jerks as a rapid movement of the zero isoline of the second derivative. From an analysis of the isoline as a function of time, they mapped the spatial extent of jerks and concluded that jerks do not appear to be worldwide. A new jerk event around 1985 was also identified in the Pacific area. Olsen & Mandea (2007) developed an approach to obtain satellite monthly means at a regular network ('virtual observatories') based on CHAMP measurements for the time period from 2001 to 2005. They detected a jerk in 2003 occurring only in a limited area near 90°E and with a stronger amplitude in the *Z* component of the magnetic field.

© 2008 The Authors
Journal compilation © 2008 RAS

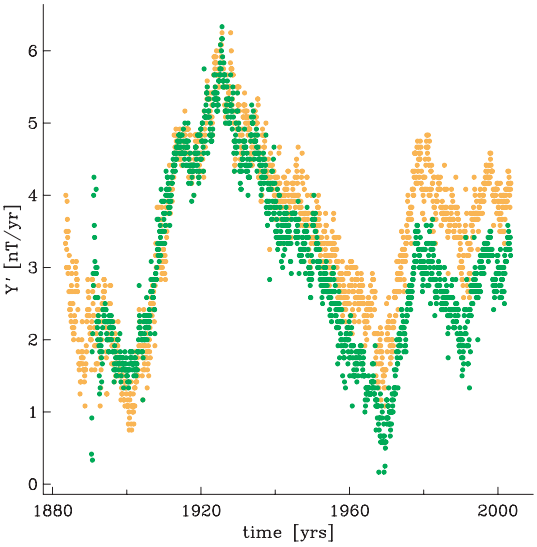

Figure 1. Secular variation of east component at Chambon la Forêt observatory in France (yellow circles) and Niemegk observatory in Germany (green circles). The data shown are first differences of observatory monthly means that have been smoothed by a 12-month running average.

The internal origin of geomagnetic jerks was demonstrated by Malin & Hodder (1982) using spherical harmonic analysis, in contradiction with other works (Alldredge 1977, 1984) that believed jerks were caused by the external field. Other recent works have confirmed the internal origin of jerks, for example, Le Huy *et al.* (1998) who performed spherical harmonic models of the 1969, 1978 and 1991 events (X, Y and Z components). In addition, Nagao *et al.* (2002) investigated geomagnetic monthly means, obtained from hourly mean values at each local time, of the three magnetic components of the same jerk. They concluded that the distribution of the jerk is independent of local time and that it cannot be explained by external currents.

Since jerks are generated in the core, they will pass through the electrical conducting mantle, before arriving at the surface. Consequently, the geomagnetic field observed at the surface will correspond to a filtered version, delayed and smoothed, of the original field generated in the core. The most relevant characteristic of geomagnetic jerks is their non-simultaneous behaviour at the earth's surface. This means that the same event occurs at slightly different times at distinct observatories (Fig. 3). We call 'differential time delays' the difference between each jerk arrival time at each observatory and a reference arrival time of the jerk (at one specific location) that can be, for example, the location where the jerk first arrived. For instance, if one observatory registered the jerk at 1968, then the differential delay of Eskdalemuir would be 1 yr and of Gnangara 4 yr (Fig. 3).

Gubbins & Tomlinson (1986) first noted a non-simultaneous behaviour of the 1969 jerk by analysing monthly means of two observatories. Later, Alexandrescu *et al.* (1996) reported a bimodal time behaviour for the 1969 and 1978 events with a clear geographical pattern of jerks first appearing in the Northern Hemisphere and later in the Southern Hemisphere, with a time lag of the order of 2 yr. Nagao *et al.* (2003) applied a statistical time-series analysis procedure to observatory data and found that the occurrence epochs of the 1969 and 1978 jerks around South Africa and South Pacific Ocean are delayed several years from those in other regions. De Michelis *et al.* (1998) analysed the 1991 jerk in data from 74 observatories and also found a non-simultaneous behaviour. Results from the comprehensive modelling approach by using the CM4 model confirmed once more that the 1969, 1978 and the 1991 jerks are not simultaneous at the Earth's surface, with time differential delays of about 2 yr (Chambodut & Mandea 2005).

The reason why jerks are not simultaneous at the Earth's surface and why there are distinct delay patterns for different jerks and magnetic components is still not well understood (Fig. 4). There are at least two simple hypotheses that could be envisaged as an explanation for this: the first is to consider these differential time delays as being generated by dynamic processes in the core which do not occur simultaneously; the second is to consider jerks generated instantaneously in the core and the time delays caused entirely by a conducting mantle.

The Earth's mantle electrical conductivity reflects chemical and

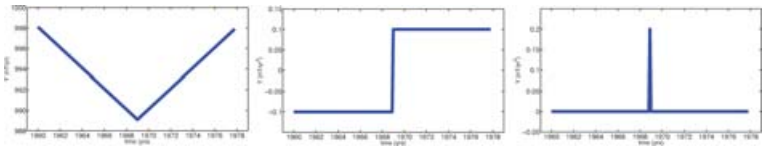

Figure 2. Simple schematic of secular variation for a hypothetic component Y. The first graph shows the typical V-shape of jerks in the secular variation. The second and third graphs show sketched the secular acceleration and the third derivative, respectively. In this case, we would have an impulse in the third derivative at the time when the jerk occurred.

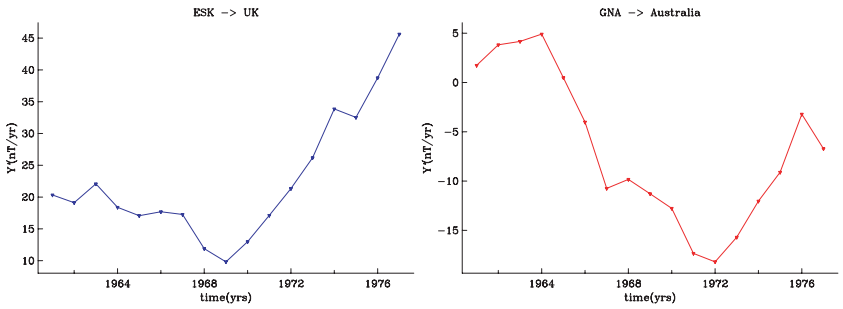

Figure 3. Secular variation (first differences of annual means) of the east component (Y) at Eskdalemuir observatory in the UK (left-hand side), where a jerk happens around 1969, and Gnangara observatory in Australia (right-hand side) where a jerk is clearly seen at around 1972.

© 2008 The Authors, *GJI*, **173,** 781–792
Journal compilation © 2008 RAS

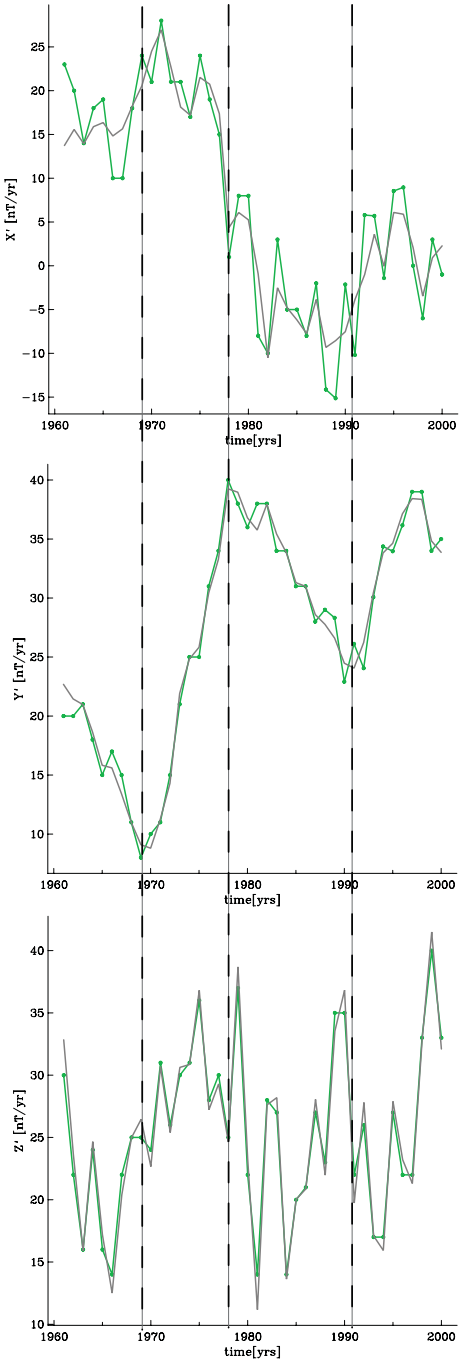

Figure 4. Secular variation of the north, east and vertical components of Niemegk observatory, in Germany. The green lines are the secular variation using annual means and the grey lines are the secular variation corrected for external and induced effects by averaging of hourly predictions from model CM4 (Sabaka *et al.* 2004).

physical properties of the planet's interior, places constraints on core–mantle coupling and controls the transmission of geomagnetic signals from the core to the surface. Temporal variations of the external magnetic field are commonly used to infer global 1-D models of the mantle's electrical conductivity. One of the earliest applications is that of Lahiri & Price (1939), who considered the general theory for any radially-varying conductivity in a spherical geometry and obtained a formal solution. They applied this theory to solar diurnal and storm-time variations to estimate the conductivities up to 1000 km depth. More recent studies such as Olsen (1999), Constable & Constable (2004) and Kuvshinov & Olsen (2006) provide estimates of the mantle conductivity. They mostly agree that electrical conductivity rises from 0.03–0.09 S m^{-1} at 400 km depth to 1–2.5 S m^{-1} at 900 km depth (Kuvshinov & Olsen 2006), but in the lowermost mantle induction studies estimates are still very uncertain due to lack of resolution. This limitation is being explored by mineral physics experiments (as Dobson & Brodholt 2000; Xu *et al.* 2000; Mao *et al.* 2004; Ono *et al.* 2006),which attempt to replicate the ambient conditions of the deep mantle. The recent discovery of post-perovskite phase change in the D″ (Iitaka *et al.* 2004; Murakami *et al.* 2004; Oganov & Ono 2004) stimulated even more the debate about the lower mantle properties. However, the results of mineral physics experiments still disagree by four orders of magnitude depending on, for example, the considered geotherm and composition. Consequently, the lower-mantle electrical conductivity is still unknown and remains as a somewhat open question.

Geomagnetic time variations generated in the core have been used in an attempt to infer some information about the mantle's electrical conductivity. Runcorn (1955) discussed the theory of the diffusion of the magnetic field by considering the mantle as an infinite sheet of uniform thickness and conductivity. He applied a step-like impulse at the bottom of the slab and evaluated what the magnetic signal observed at the top would be. Achache *et al.* (1980) performed the same calculation but they use instead a ramp-function at the bottom of the slab, assumed to be 2000 km thick. They calculated responses for different values of electrical conductivity, and based on the 1969 jerk, they estimated the average conductivity of the slab as being 60 S m^{-1}.

More recently, Alexandrescu *et al.* (1999) assumed a jerk as a pure singularity at the core–mantle boundary (CMB) and evaluated the effect caused by a uniformly conducting mantle. The estimated electrical conductivity is less than 10 S m^{-1} on average assuming a uniform conducting lower mantle, 2000 km thick, and an insulating upper mantle. Nagao *et al.* (2003) also solved the diffusion equation in the mantle for an abrupt change occurring simultaneously at the CMB. They believe that the later arrival of jerks in South Africa and South Pacific Ocean may be explained by higher conductivities beneath these regions. The electrical conductivity is assumed to be constant apart from anomalies around South Africa and the South Pacific Ocean. There is a contradiction between the estimated conductivity in the region of South Africa by the delay times (>200 S m^{-1}) and by the duration time of jerks (<40 S m^{-1}). The duration of the jerk is the time it takes for the change in the slope to be accomplished, and is very difficult to measure in the data due to the presence of noise. In addition, if there are higher conductivities under South Africa and the South Pacific Ocean, all jerks would be late in these regions, a feature not seen in 1991.

In this paper, we analyse the hypothesis that jerks are simultaneous at the CMB and that the delays are entirely caused by a conducting mantle. We assume a jerk to be an impulse in time at the CMB with a morphology given by two synthetic models. A summary of Backus' (1983) theory is given in Section 2 and applied to arbitrary 1-D mantle electrical conductivity models to illustrate the physical effect of the mantle filter. Synthetic models of jerk amplitudes of the north, east and vertical components of the magnetic field are presented in Section 3, where we demonstrate that a 1-D mantle conductivity model is able to generate differential jerk time delays at the Earth's surface due to the mixing of harmonics. In this respect it is not necessary to invoke laterally varying conductivity to generate differential delays in different regions. In addition, since the jerk morphology varies for different magnetic components, the

© 2008 The Authors, *GJI*, **173,** 781–792
Journal compilation © 2008 RAS

differential time delays at the Earth's surface also do so. We apply this theory to a real morphology of a jerk taken from Le Huy *et al.*'s (1998) spherical harmonic analysis of the 1969 jerk (Section 4). The resulting differential time delays that would be seen in a realistic distribution of observatories is shown. This also leads to the conclusion that since jerk morphologies are different in distinct jerk events, then the pattern of differential time delays will also change as a function of the particular event.

2 THEORY

To explore the hypothesis that jerk differential time delays are generated entirely by the electrically conducting mantle, the Earth is modelled as a linear filter system—the input is represented by temporal and a spatial part of the jerk at the CMB, the filter originates from the properties of the electrically conducting mantle, and the output is the jerk observed at the Earth's surface. We assume that the jerk is simultaneously generated at the CMB and simulated as an impulse in the third time-derivative of the geomagnetic field. The diffusive effect of the mantle is illustrated by a simple 1-D radial conductivity model $\sigma(r)$.

The transmission of the magnetic field from the core to the surface is governed by the diffusion equation. For a non-uniform conductor, the diffusion equation is written as,

$$\frac{\partial \mathbf{B}}{\partial t} = -\nabla \times (\eta \nabla \times \mathbf{B}), \tag{1}$$

where $\mathbf{B}$ is the magnetic field and we consider the magnetic diffusivity η as a function of the radius $\eta = \eta(r) = \frac{1}{\mu_0 \sigma(r)}$.

The appropriate way to solve the diffusion equation when the conductor has a spherical symmetry with a radial conductivity dependence is by using a toroidal–poloidal decomposition of the magnetic field (Gubbins & Roberts 1987),

$$\mathbf{B} = \mathbf{B}_t + \mathbf{B}_p, \tag{2}$$

the vectors $\mathbf{B}_t$ and $\mathbf{B}_p$ are called the toroidal and poloidal magnetic fields, respectively, and can be written in terms of poloidal and toroidal scalars [$\mathcal{P}(r, \theta, \phi, t)$ and $\mathcal{T}(r, \theta, \phi, t)$],

$$\mathbf{B} = \nabla \times [\mathcal{T}(r, \theta, \phi, t)\mathbf{r}] + \nabla \times \nabla \times [\mathcal{P}(r, \theta, \phi, t)\mathbf{r}], \tag{3}$$

where $\mathbf{r}$ is the radius vector from the geocentre, θ is the colatitude and ϕ the longitude. Only the relation between the poloidal magnetic field at the CMB ($r = c = 3485$ km) and at the Earth's surface ($r = a = 6371$ km) is considered in this paper, since the toroidal magnetic fields are absent in the region $r > a$ because of the insulating atmosphere. In short hand notation $\mathcal{P} = \mathcal{P}(r, \theta, \phi, t)$ and the magnetic field $\mathbf{B}$ in eq. (3) can be written as

$$\mathbf{B} = \nabla \times \nabla \times (\mathcal{P}\mathbf{r}) = \nabla \left[\frac{\partial}{\partial r}(r\mathcal{P}) \right] - \mathbf{r}\nabla^2 \mathcal{P}, \tag{4}$$

and the curl of the magnetic field will be:

$$\nabla \times \mathbf{B} = \nabla \times \left[(-\nabla^2 \mathcal{P})\mathbf{r} \right]. \tag{5}$$

Substituting eqs (4) and (5) into (1) we obtain the diffusion equation for the poloidal scalar:

$$\frac{\partial \mathcal{P}}{\partial t} = \frac{1}{\mu_0 \sigma(r)} \nabla^2 \mathcal{P}, \tag{6}$$

which can be rewritten in terms of spherical harmonics, since the poloidal scalar $\mathcal{P}$ can be expanded as

$$\mathcal{P} = \sum_{\ell=1}^{\infty} \sum_{m=-\ell}^{\ell} p_\ell^m(r, t) Y_\ell^m(\theta, \phi), \tag{7}$$

where $p_\ell^m(r, t)$ are functions in the spherical harmonic decomposition, ℓ is the degree, m the order and Y_ℓ^m the Schmidt quasi-normalized spherical harmonics. If the Laplacian is represented by

$$\nabla^2(.) = \frac{1}{r} \frac{\partial^2}{\partial r^2}[r(.)] - \frac{L^2(.)}{r^2}, \tag{8}$$

and the operator L^2 applied to spherical harmonics is

$$L^2 Y_\ell^m(\theta, \phi) = \ell(\ell + 1) Y_\ell^m(\theta, \phi), \tag{9}$$

we can rewrite eq. (6) in the form

$$\frac{\partial p_\ell^m(r, t)}{\partial t} = \frac{1}{\mu_0 \sigma(r)} \left(\frac{1}{r} \frac{\partial^2}{\partial r^2} \left(r p_\ell^m(r, t) \right) - \frac{l(l + 1)}{r^2} p_\ell^m(r, t) \right). \tag{10}$$

To solve the diffusion equation in the frequency domain, one must define the Fourier transform of the poloidal scalar

$$\tilde{\mathcal{P}}(r, \theta, \phi, \omega) = \int_{-\infty}^{\infty} \mathcal{P}(r, \theta, \phi, t) e^{\imath \omega t} \, \mathrm{d}t, \tag{11}$$

and its inverse Fourier transform as

$$\mathcal{P}(r, \theta, \phi, t) = \frac{1}{2\pi} \int_{-\infty}^{\infty} \tilde{\mathcal{P}}(r, \theta, \phi, \omega) e^{-\imath \omega t} \, \mathrm{d}\omega. \tag{12}$$

The Fourier equivalent to the poloidal scalar diffusion eq. (6) is

$$\tilde{\mathcal{P}} = -\frac{1}{\imath \omega \mu_0 \sigma(r)} \nabla^2 \tilde{\mathcal{P}}, \tag{13}$$

or in terms of spherical harmonics (Fourier transform of eq. 10):

$$\tilde{p}_\ell^m(r, \omega) = -\frac{1}{\imath \omega \mu_0 \sigma(r) r} \left\{ \frac{\partial^2}{\partial r^2} \left[r \tilde{p}_\ell^m(r, \omega) \right] - \frac{\ell(\ell + 1)}{r} \tilde{p}_\ell^m(r, \omega) \right\}. \tag{14}$$

To illustrate the effect of an electrical conductor we adopt a 1-D mantle model that increases with depth as used by Lahiri & Price (1939):

$$\sigma(r) = \sigma_c \left(\frac{c}{r} \right)^{2\gamma + 2}, \tag{15}$$

where σ_c is the electrical conductivity at the CMB and γ a positive constant. Two radial models are created, following eq. (15): the first is a weaker conducting model with $\sigma_c = 100$ S m^{-1} and $\gamma = 8$ and the second a very strong conductor with $\sigma_c = 3000$ and $\gamma = 11$, both shown in Fig. 5.

In the weakly conducting model, the electrical conductivity at the surface is 0.0019 and 0.0416 S m^{-1} at 1000 km depth, while the highly conducting model goes from 0.0015 S m^{-1} at the surface up to 0.0930 S m^{-1} at 1000 km. It is clear that both are not realistic models for the Earth, but instead they are used to illustrate two issues: how the delay times depend on the conductivity and how a 1-D mantle conductivity model can cause differential time delays at the Earth's surface.

By defining,

$$\nu = \frac{1}{\gamma}(\ell + 0.5) \tag{16}$$

and

$$z_r = \frac{1}{\gamma} (\imath \omega \mu_0 \sigma_c c^2)^{1/2} \left(\frac{c}{r} \right)^{\gamma}, \tag{17}$$

and assuming the radial mantle conductivity model in eq. (15), Gubbins & Roberts (1987) show how eq. (14) reduces to Bessel's equation, given by

$$\frac{\partial^2 f(z)}{\partial z^2} + \frac{1}{z} \frac{\partial f(z)}{\partial z} + \left(1 - \frac{\nu^2}{z^2} \right) f(z) = 0, \tag{18}$$

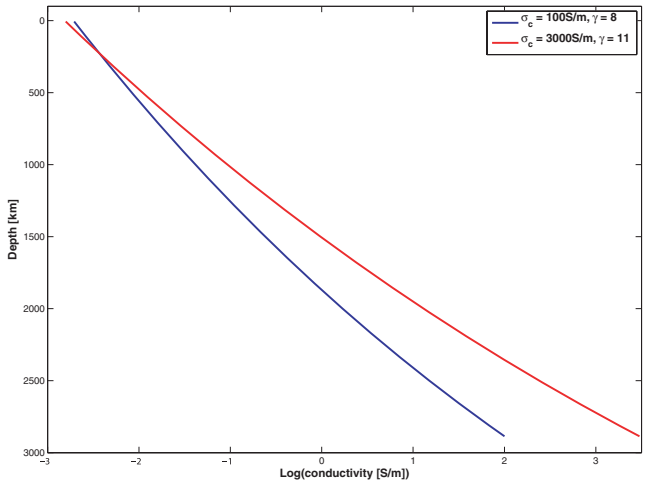

Figure 5. Radial models of mantle electrical conductivity (eq. 15): the blue curve represents a weakly conducting model and the red curve a highly conducting model.

of order ν for $f(z) = r^{\frac{1}{2}}\widetilde{p}_\ell^m(r,\omega)$. We suppose that γ is so large that the electrical conductivity falls rapidly to zero with increasing r, being zero before $r = a$ is reached. Since $r = \infty$ corresponds to $z_\infty = 0$ (eq. 17), the Bessel function should vanish at $z = 0$, consequently $f(z) = J_\nu(z)$, where J_ν is the Bessel function of order ν.

If we let $\widetilde{p}_\ell^m(r,\omega) = r^{-\frac{1}{2}}J_\nu(z_r)$ be the solution of equation (14), for any fixed harmonic degree (ℓ), $\widetilde{p}_\ell^m(c,\omega)$ can be regarded as the input to the mantle which produces output $\widetilde{p}_\ell^m(a,\omega)$ at the Earth's surface. In the frequency domain, any input and output functions can be related by

$$\widetilde{p}_\ell^m(a,\omega) = \mathcal{G}_\ell \tilde{F}_\ell(\omega)\widetilde{p}_\ell^m(c,\omega), \tag{19}$$

where $\mathcal{G}_\ell$ is the geometrical attenuation,

$$\mathcal{G}_\ell = \left(\frac{c}{a}\right)^{\ell+1}, \tag{20}$$

and $\tilde{F}_\ell(\omega)$ is the transfer function given by

$$\tilde{F}_\ell(\omega) = \left(\frac{z_c}{z_a}\right)^{\nu}\frac{J_\nu(z_a)}{J_\nu(z_c)}. \tag{21}$$

Note that the mantle filter can be described as a combination of geometrical and electromagnetic filters, that depend on the electrical conductivity and on the spherical harmonic degree ℓ, but not on the order m.

In the time domain the output is evaluated by the convolution (denoted$*$) of the input with the mantle filter:

$$\begin{aligned} p_\ell^m(a,t) &= \mathcal{G}_\ell F_\ell(t) * p_\ell^m(c,t) \\ &= \mathcal{G}_\ell \int_{-\infty}^{\infty} F_\ell(t-t')p_\ell^m(c,t')\,\mathrm{d}t', \end{aligned} \tag{22}$$

where $F_\ell(t)$ is the impulse response function (IRF). The Transfer Function and the IRF are related by the Fourier transform,

$$\tilde{F}_\ell(\omega) = \int_{-\infty}^{\infty} F_\ell(t)e^{\imath\omega t}\,\mathrm{d}t, \tag{23}$$

and for zero frequency, $\omega = 0$,

$$\tilde{F}_\ell(0) = \int_{-\infty}^{\infty} F_\ell(t)\,\mathrm{d}t, \tag{24}$$

which is the area under the IRF curve. We use the same convention as Backus (1983) that $\int_{-\infty}^{\infty} F_\ell(t)\,\mathrm{d}t = 1$.

Backus (1983) demonstrated that if the electrical conductivity of the mantle depends only on radius [$\sigma(r)$], the mantle behaves as a causal, time-invariant, real and linear filter. There are two constants characterizing this filter for each harmonic degree; the delay time

$$\tau_\ell = \frac{1}{\tilde{F}_\ell(0)}\int_{-\infty}^{\infty} F_\ell(t)t\,\mathrm{d}t, \tag{25}$$

evaluated from the first moment of the IRF curve, and the smoothing time:

$$\alpha_\ell = \frac{1}{\tilde{F}_\ell(0)}\int_{-\infty}^{\infty} F_\ell(t)(t-\tau_\ell)^2\,\mathrm{d}t, \tag{26}$$

equivalent to the second central moment of the IRF.

For the two radial mantle models (Fig. 5) we evaluated the IRF for different harmonic degrees (Fig. 6) and their delay times and smoothing (eqs 25 and 26). The most conducting model suffers more delay and smoothing by the mantle: the delay time is of the order of 2.5 yr for $\ell = 1$ and for the less conducting one, the delay time is about 55 d for the same harmonic degree. One of the most important points is that smaller harmonic degrees suffer more delay and smoothing than higher harmonic degrees. Fig. 6 shows that for the weaker conducting model, the time delay for $\ell = 1$ is about 55 d while for $\ell = 5$ it is of the order of 40 d.

3 SYNTHETIC MODELS

One of the characteristics of geomagnetic jerks that is not completely understood is that the jerk arrival times are not the same for each component of the magnetic field. To illustrate this, Fig. 4 shows the secular variation of the north, east and vertical components of Niemegk observatory where the 1969 jerk occurs at slightly different times. It is also important to note that the jerks will be usually better seen in the east component because it suffers less influence of the magnetospheric field. In addition, the jerk time detection will depend on the method applied, as for example, if it is detected by the fitting of two straight lines or by more sophisticated methods, such as wavelet analysis.

Jerk amplitudes are measured at the Earth's surface [$\mathcal{A}(a,\theta,\phi)$], at magnetic observatories, and used to build global spherical harmonic models:

$$\mathcal{A}(a,\theta,\phi) = \sum_{\ell=1}^{L}\sum_{m=0}^{\ell=1}\mathcal{A}_\ell^m(a,\theta,\phi). \tag{27}$$

One important issue is that each component of the magnetic field [$X(a,\theta,\phi)$, $Y(a,\theta,\phi)$ and $Z(a,\theta,\phi)$] presents a different jerk morphology [notation $\mathcal{X}(a,\theta,\phi)$, $\mathcal{Y}(a,\theta,\phi)$ and $\mathcal{Z}(a,\theta,\phi)$ for jerk amplitudes] since they represent components of the gradient of the potential ($\mathcal{V}$):

$$\mathcal{X} = -\frac{1}{r}\frac{\partial\mathcal{V}}{\partial\theta}, \qquad \mathcal{Y} = \frac{1}{r\sin\theta}\frac{\partial\mathcal{V}}{\partial\phi}, \qquad \mathcal{Z} = -\frac{\partial\mathcal{V}}{\partial r},$$

where the potential can be expanded in spherical harmonics:

$$\begin{aligned} \mathcal{V}(a,\theta,\phi) = a\sum_{\ell=1}^{L}\sum_{m=0}^{\ell=1}\left(\frac{a}{r}\right)^{\ell+1}&\left(\delta\ddot{g}_\ell^m\cos m\phi + \delta\ddot{h}_\ell^m\sin m\phi\right) \\ &\times P_\ell^m(\cos\theta) \end{aligned}$$

and the coefficients $\delta\ddot{g}_l^m$ and $\delta\ddot{h}_l^m$ are in nT yr^{-2}. We consider two

© 2008 The Authors, *GJI*, **173,** 781–792
Journal compilation © 2008 RAS

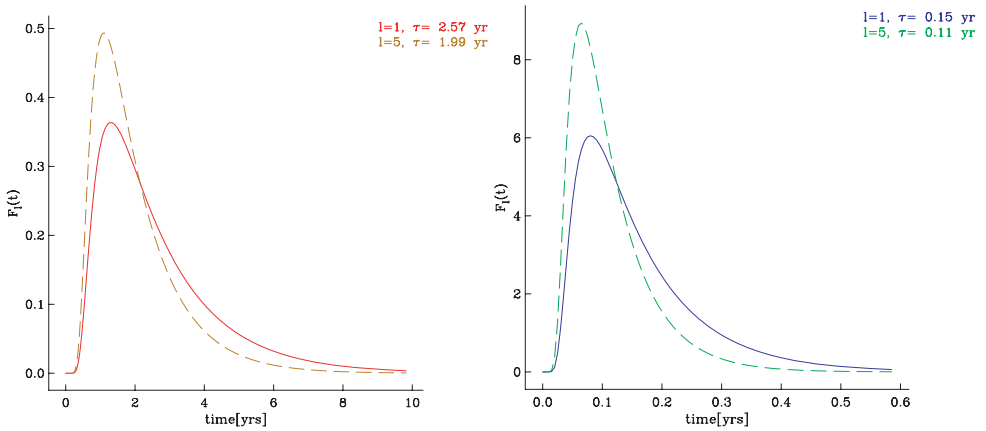

Figure 6. Impulse Response functions for the two electrical radial conductivity models, shown in eq. (15). The left plot corresponds to the higher conducting model ($\sigma_c = 3000$ and $\gamma = 11$) and the right plot to the weaker conducting model ($\sigma_c = 100$ and $\gamma = 8$).

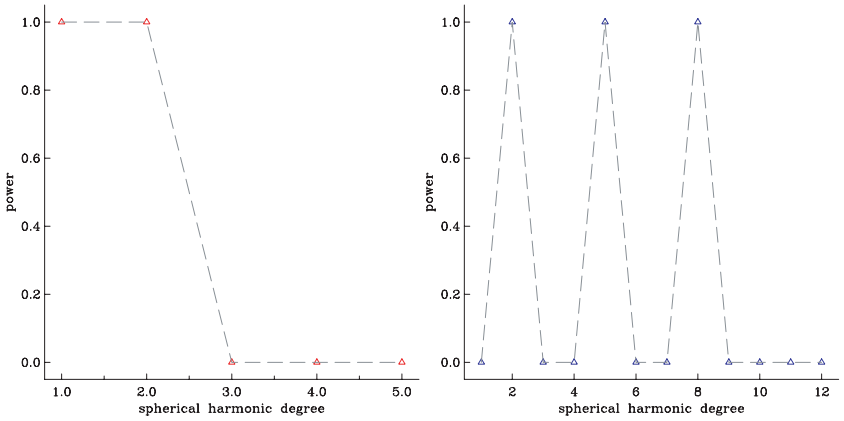

Figure 7. Power Spectrum of the two synthetic model of jerk amplitudes.

synthetic models defined in terms of their Lowes spatial power spectrum:

$$R_\ell = (\ell+1)\sum_{m=0}^{\ell}\left[\left(\delta\ddot{g}_\ell^m\right)^2 + \left(\delta\ddot{h}_\ell^m\right)^2\right], \tag{28}$$

The first model has two peaks at $\ell = 1$ and $\ell = 2$ with a truncation degree $L = 2$, while the second model presents three peaks at $\ell = 2$, 5 and 8 and $L = 8$ (Fig. 7). Both models were built with a power spectrum with peaks of $R_\ell = 1$, where each coefficient ($\delta\ddot{g}_\ell^m$ and $\ddot{h}_\ell^m$) of each harmonic degree has the same value. For example, in the case of the two peaked model, the three non-zero coefficients of $\ell = 1$ are all equal to 0.40825 and the five non-zero coefficients of $\ell = 2$ are equal to 0.25820 which gives as a result two peaks $R_1 = 1$ and $R_2 = 1$. The synthetic spherical harmonic models are shown in Fig. 8 for the north (X), east (Y) and vertical (Z) components of the magnetic field. We used as an example the highly conducting model in Fig. 5 ($\sigma_c = 3000$ and $\gamma = 11$) and calculated the time delays of the two synthetic morphology models (Fig. 9). It is clear that the patterns of time delays of X, Y and Z components are different depending on their morphologies. This would explain why jerks are not seen at the same time in different components. If there is more mixing of harmonics, the jerk morphology will be more complex as also will be the pattern of time delays (see comparison in Fig. 9).

4 GEOPHYSICAL APPLICATION

Let the input be written in a general form as $\delta\ddot{p}_\ell^m(c,t) = \delta(t)\mathcal{A}_\ell^m(c,\theta,\phi)$, where $\delta(t)$ is the Dirac delta function, and eq. (22) becomes:

$$\begin{aligned}\delta\ddot{p}_\ell^m(a,t)Y_\ell^m(\theta,\phi) &= \mathcal{G}_\ell\mathcal{A}_\ell^m(c,\theta,\phi)\int_{-\infty}^{\infty}F_\ell(t-t')\delta(t')\,dt' \\ &= \mathcal{G}_\ell\mathcal{A}_\ell^m(c,\theta,\phi)F_\ell(t).\end{aligned} \tag{29}$$

Spherical harmonic models are constructed by using measurements of jerk amplitudes at the Earth's surface. However, to obtain the input model at the CMB [$\mathcal{A}_\ell^m(c,\theta,\phi)$], the mantle is assumed initially to be an insulator and a downwards continuation, from the surface to the CMB, is applied:

$$\mathcal{A}_\ell^m(c,\theta,\phi) = \mathcal{A}_\ell^m(a,\theta,\phi)\left(\frac{a}{c}\right)^{(\ell+1)}. \tag{30}$$

There is no inconsistency in considering at first the mantle as an insulator and then in solving the forward problem assuming a mantle as a conductor. The reason is that the mantle filter does not modify jerk amplitudes because $\int_{-\infty}^{\infty}F_\ell(t)\,\mathrm{d}t = 1$, it only delays and smoothes the input jerk. In addition, when we convolve the input with the IRF (eq. 29), an upward continuation or geometrical attenuation ($\mathcal{G}_\ell$) is applied. Therefore, both downward and upward

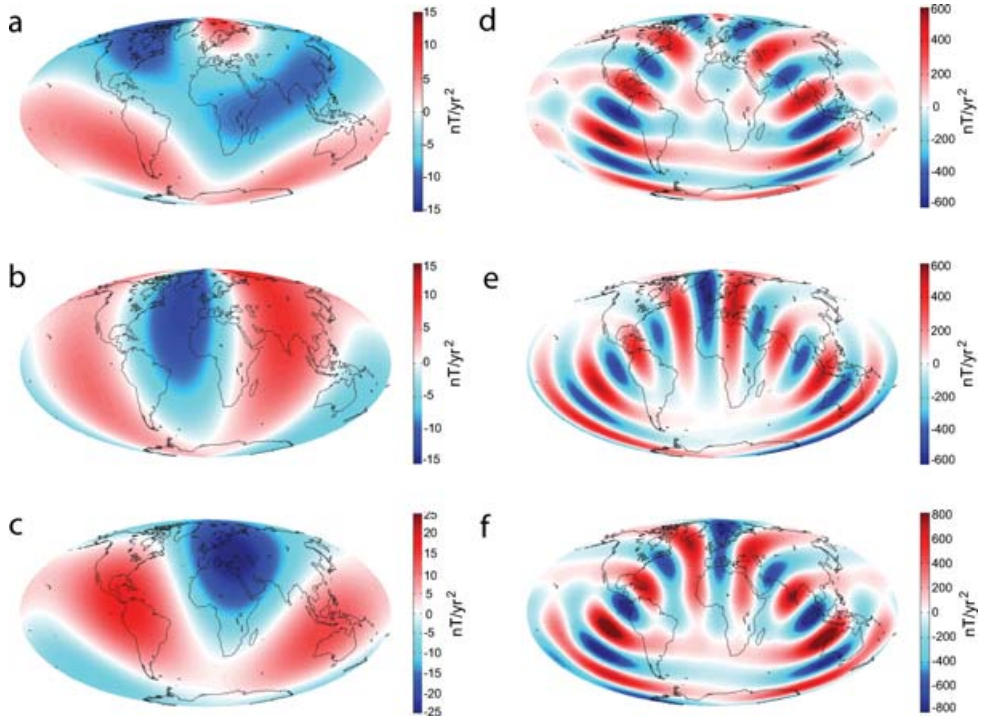

Figure 8. Synthetic spherical harmonic models evaluated from the synthetic models (Fig. 7) at the core–mantle boundary. The synthetic model with two peaks in the power spectrum is shown in (a) for the north component of the magnetic field (X), in (b) for the east component (Y) and in (c) for the vertical component (Z). The three peaked synthetic model is shown in (d) for X, in (e) for Y and in (f) for Z. The colour scale in in nT yr^{-2}.

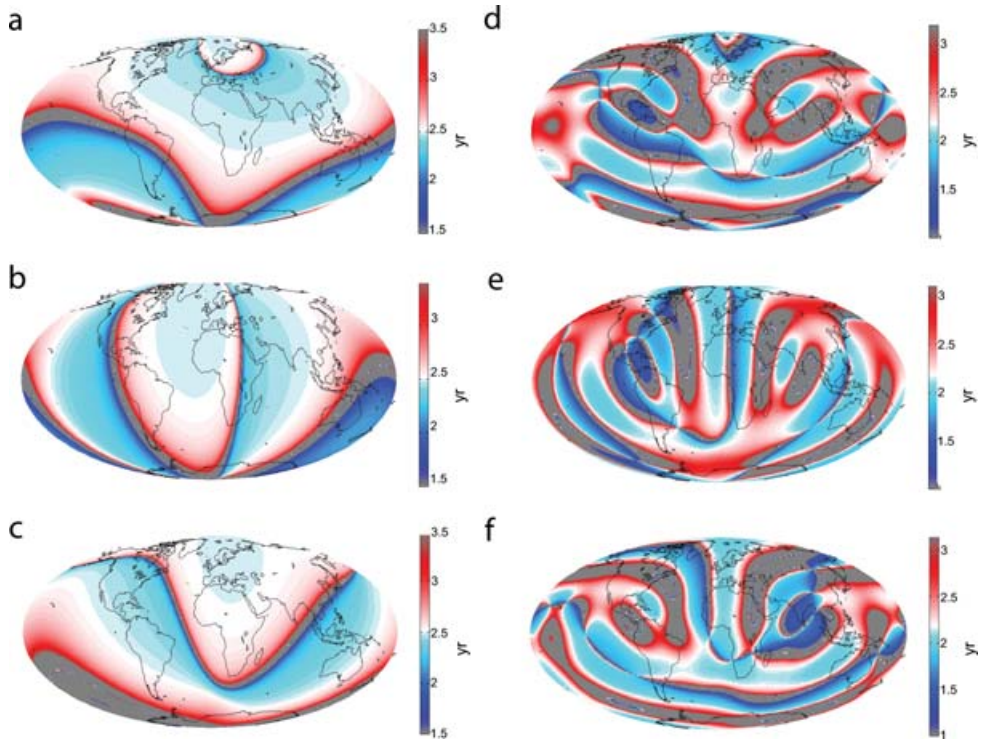

Figure 9. Results of the forward modelling calculation of time delays for the two-peaked model (a, b, c) and for the three-peaked model (d, e, f) by using the highly conducting model. In (a) and (d) the time delays are for the north component of the magnetic field (X), in (b) and (e) for the east component (Y) and in (c) and (f) for the vertical component (Z). The colour scale is in years and the red would mean late jerks, while the blue earlier jerks. The areas with grey colour correspond to locations where the time delay could not be detected because of zero jerk amplitude (see Fig. 8).

© 2008 The Authors, *GJI*, **173,** 781–792
Journal compilation © 2008 RAS

continuations cancel out. By using eqs (29) and (30):

$$\begin{aligned}\delta\ddot{p}_\ell^m(a,t)Y_\ell^m(\theta,\phi) &= \left(\frac{c}{a}\right)^{\ell+1}\mathcal{A}_\ell^m(c,\theta,\phi)F_\ell(t)\\ &= \left(\frac{c}{a}\right)^{\ell+1}\mathcal{A}_\ell^m(a,\theta,\phi)\left(\frac{a}{c}\right)^{(\ell+1)}F_\ell(t)\\ &= \mathcal{A}_\ell^m(a,\theta,\phi)F_\ell(t).\end{aligned} \tag{31}$$

This means that to solve the forward problem we can use the spherical harmonic model of jerk amplitudes at the surface $[\mathcal{A}_\ell^m(a,\theta,\phi)]$ and ignore the geometrical attenuation, instead of using the model at the CMB.

In this section, Backus' (1983) mantle filter theory is applied to two real geomagnetic jerk morphologies (east component) of the 1969 jerk taken from Le Huy *et al.* (1998) who analysed 123 observatories and of the 2003 jerk taken from Olsen & Mandea (2007) who used CHAMP satellite data (Figs 10 and 11). The truncation degree used by Le Huy *et al.* (1998) was taken as $L = 4$, and for each spherical harmonic degree we evaluated the associated jerk amplitude model (Fig. 10), while for Olsen & Mandea

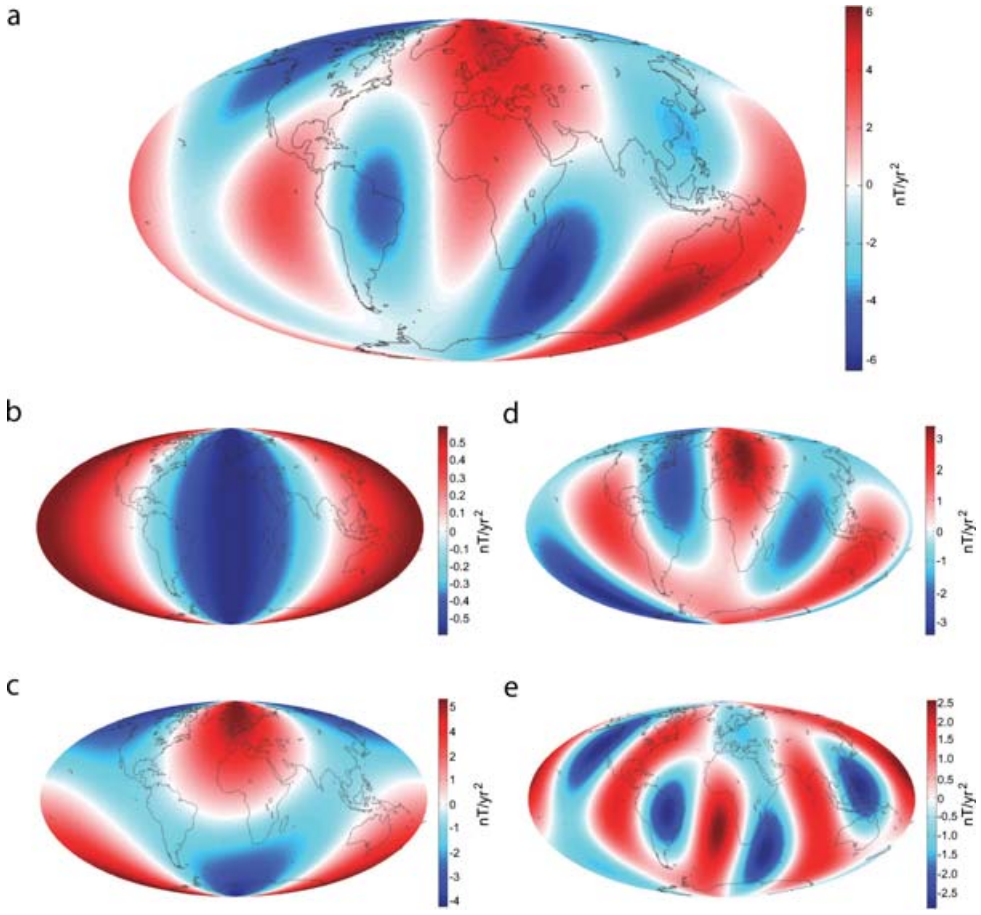

Figure 10. Spherical harmonic model obtained from Le Huy *et al.* (1998) of the east component of the 1969 geomagnetic jerk at the Earth's surface (a). Spherical harmonic models of each harmonic degree at the Earth's surface for: $\ell = 1$ (b), $\ell = 2$ (c), $\ell = 3$ (d) and $\ell = 4$ (e).

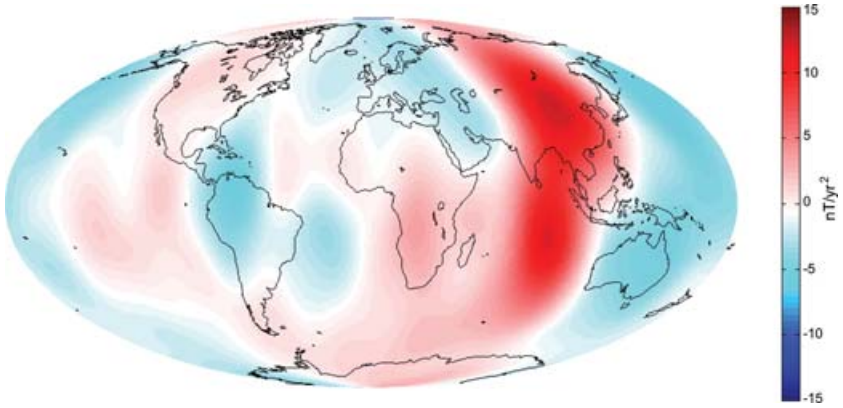

Figure 11. Morphology of the 2003 geomagnetic jerk for the east component obtained from Olsen & Mandea (2007). Their model is truncated to spherical harmonic degree $L = 14$.

© 2008 The Authors, *GJI*, **173,** 781–792
Journal compilation © 2008 RAS

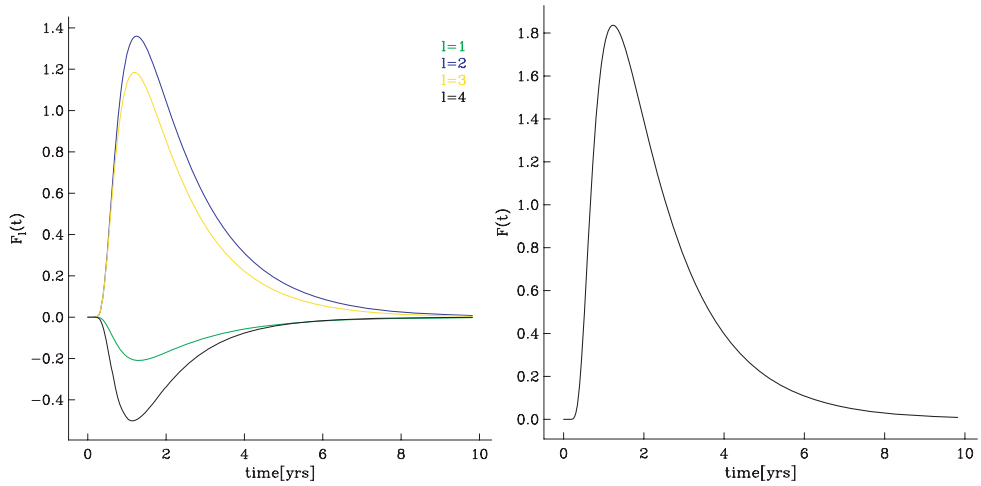

Figure 12. In (a) the Impulse Response Function multiplied by the amplitude value for each harmonic degree (ℓ), of the location corresponding to L'Aquila magnetic observatory (Italy). By comparison with Fig. 10 it is possible to check that in Italy, for $\ell = 1$ and $\ell = 4$ the amplitudes are negative, while for $\ell = 2$ and $\ell = 3$ the amplitudes are positive. The sum of these curves result in the Composite Impulse Response Function (b).

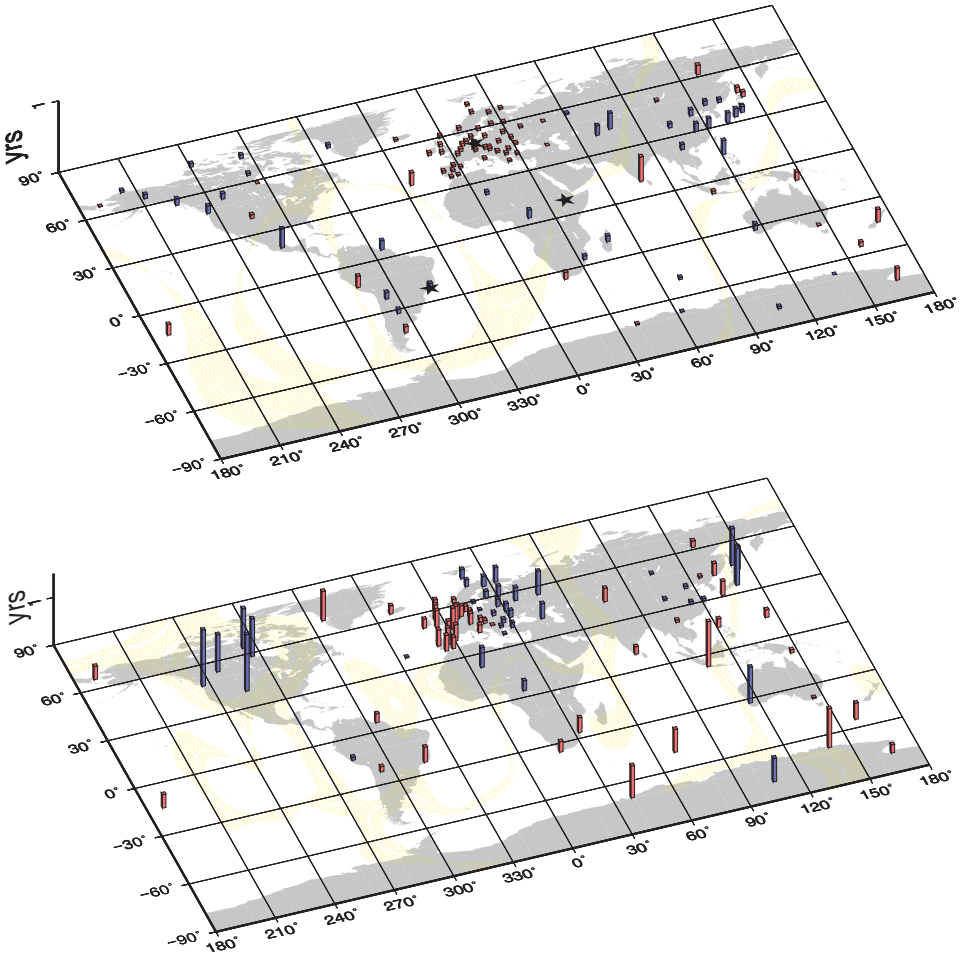

Figure 13. Results of the forward model for time delays of the 1969 jerk of the *Y* component using Le Huy *et al.* (1998) spherical harmonic model of the 1969 jerk (Fig. 10) on the top map with a mean time delay of 2.289 yr and Olsen & Mandea (2007) model for the 2003 jerk (Fig. 11) with a mean time delay of 2.252 yr on the bottom map. In both models a highly electrically conducting mantle model (Fig. 5) was used. The yellow areas correspond to extremely high time delay values, blue bars represent early jerks where the time delay shown on the vertical scale is to be subtracted from the average and red bars are late jerks, where the values of the vertical scale are to be added to the average. The stars are at the location of observatories used as example in Fig. 14.

© 2008 The Authors, *GJI*, **173,** 781–792
Journal compilation © 2008 RAS

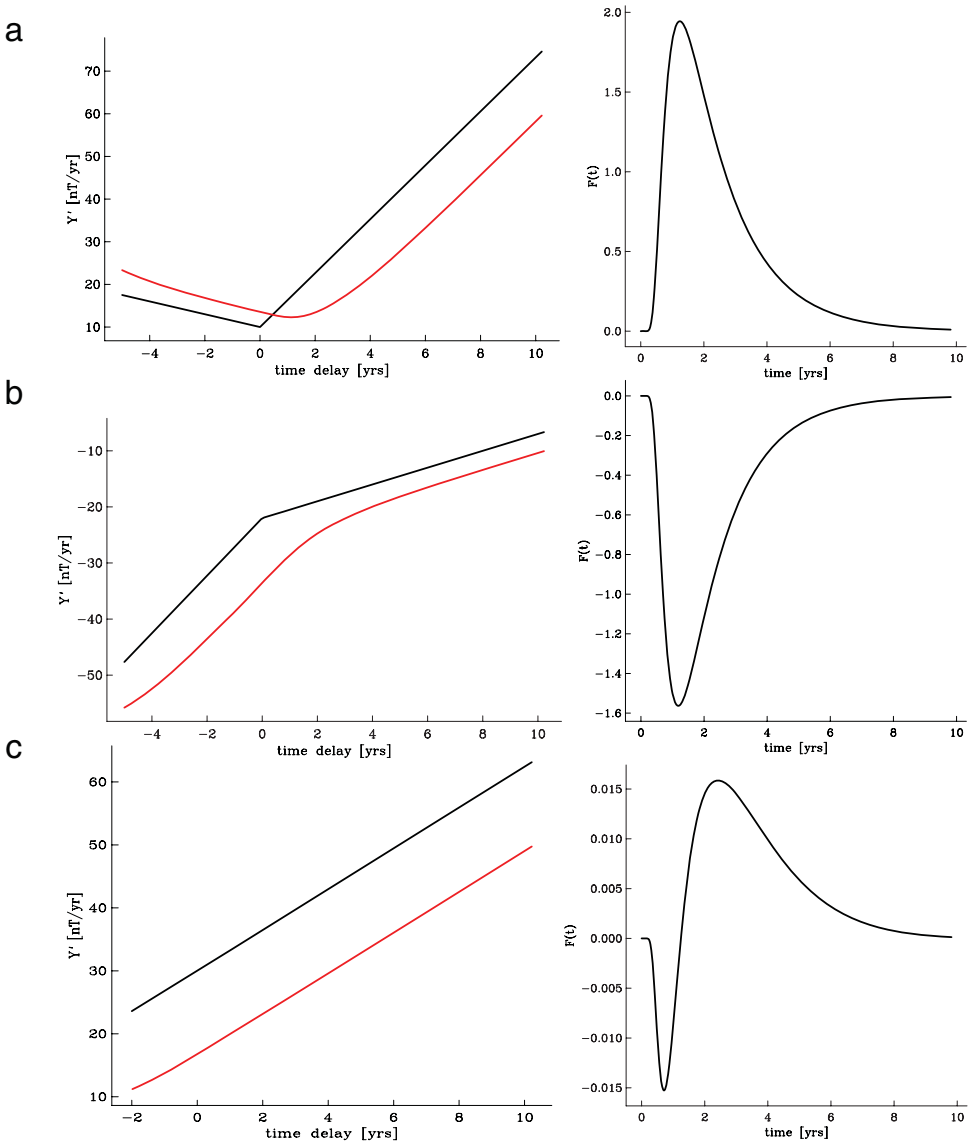

Figure 14. Synthetic jerks in the case of an insulating mantle (black 'V' shape) and in the case of a conducting mantle (red line), which is the result of the convolution between the CIRF of each observatory (in the right column) and the input jerk at the CMB. These results consider a high mantle electrical conductivity model (in Fig. 5 for $\sigma_c = 3000$ and $\gamma = 11$) and the jerk morphology of Le Huy *et al.* (1998) (in Fig. 10). Different observatory locations are considered to illustrate the delay and smoothing caused by a hypothetic electrical conducting mantle: (a) Niemegk with a positive CIRF, (b) Vassouras with a negative CIRF and (c) Addis Ababa (AAE) with an oscillatory CIRF. The amplitudes of these hypothetic jerks are roughly the same as the real ones.

(2007) the truncation degree was taken as $L = 14$. Conversely, we assume an unrealistic highly conducting model for the mantle, as shown in Fig. 5. The aim of this section is to demonstrate that the same arbitrary 1-D electrical model is able to generate differential time delays at the surface at a realistic distribution of observatories.

By having both jerk amplitudes and IRF for each ℓ we can introduce the Composite Impulse Response Function [CIRF, $F(r, \theta, \phi, t)$, in short notation $F(t)$], which is the sum of the IRF [$F_\ell(t)$] multiplied by jerk amplitudes [$\mathcal{A}_\ell^m(r, \theta, \phi)$], for each harmonic degree:

$$F(t) = \sum_{\ell=1}^{L} \sum_{m=0}^{\ell} \mathcal{A}_\ell^m(a, \theta, \phi) F_\ell(t). \tag{32}$$

It is obvious that since jerk amplitudes vary spatially, the CIRFs will also do so (eq. 32). If we look at one observatory location for Le Huy *et al.*'s model, for example L'Aquila Observatory (Italy), we can note how a CIRF is generated by the linear combination of the IRFs multiplied by the amplitude of that location, for each ℓ (Fig. 12).

By evaluating the CIRF of each location we can measure its delay time by combining eqs (25) and (32):

$$\begin{aligned} \tau &= \frac{1}{\tilde{F}(0)} \int_{-\infty}^{\infty} F(t) t \, \mathrm{d}t \\ &= \frac{1}{\tilde{F}(0)} \sum_{\ell=1}^{L} \sum_{m=0}^{\ell} \mathcal{A}_\ell^m(r, \theta, \phi) \int_{-\infty}^{\infty} F_\ell(t) t \, \mathrm{d}t \\ &= \frac{1}{\tilde{F}(0)} \sum_{\ell=1}^{L} \tau_\ell \sum_{m=0}^{\ell} \mathcal{A}_\ell^m(r, \theta, \phi), \end{aligned} \tag{33}$$

© 2008 The Authors, *GJI*, **173,** 781–792
Journal compilation © 2008 RAS

where,

$$\tilde{F}(0) = \int_{-\infty}^{\infty} F(t)\,\mathrm{d}t = \sum_{\ell=1}^{L}\sum_{m=0}^{\ell} \mathcal{A}_\ell^m(r,\theta,\phi)\int_{-\infty}^{\infty} F_\ell(t)\,\mathrm{d}t = \sum_{\ell=1}^{L}\sum_{m=0}^{\ell} \mathcal{A}_\ell^m(r,\theta,\phi). \quad (34)$$

As the CIRFs vary spatially it is a straightforward conclusion that time delays (τ) will also be different at each location (eq. 33). We can then evaluate τ, using Le Huy *et al.*'s (1998) spherical model and the same 1-D highly conducting mantle model (Figs 10 and 5), in different locations. The result is presented in Fig. 13 for a typical distribution of observatories, where the blue bars would correspond to early jerks and red bars to late jerks. For instance, in Europe the bars are small because the time delay values are close to the mean delay time. In this example, the differential delays are of the order of 2 yr (see vertical scale in Fig. 13). However, it is important to stress that these results should not be compared with real differential delays measured in observatories because we are assuming an arbitrary mantle electrical model and also because small changes in the spherical harmonic model of jerk amplitudes can cause substantial differences in the pattern of time delays. We also applied the high conducting mantle model to the 2003 jerk morphology (Y component) and we found differential time delays of the order of 3 yr. The 2003 jerk was reported to be concentrated near 90°E, with maximum jerk strength at about ±30° latitude and with small differential time delays of the order of a month. By the application of this forward approach we found also very small differential delays in this area.

Some examples of CIRF and the resulting jerk at the surface are shown in Fig. 14 for the location corresponding to the three observatories shown in Fig. 13. The extremely high values of time delays (yellow area in Fig. 13) are caused by an oscillatory CIRF, as shown in Fig. 14 for the location corresponding to Addis Ababa (AAE) observatory. The estimated time delays in oscillatory CIRFs have extremely high values because when the area under the CIRF curve is close to zero [$\tilde{F}(0) \sim 0$] then τ values will be also extremely high (see eq. 33). These anomalous values of time delays coincide with locations of zero amplitude shown by Le Huy *et al.* (1998) spherical harmonic model (Fig. 10). Locations of jerk zero amplitude would mean that the jerk could not be observed and therefore time delays could not be measured.

5 CONCLUSION

We applied Backus' (1983) mantle filter theory and verified that the mantle filter acts differently on each harmonic degree. The mixing of harmonics varies with location, depending on the jerk morphology at the Earth's surface. As a consequence, the arrival times of geomagnetic jerks that are measured by the first moment of the composite impulse response curve, will be different at each location. To illustrate that, we used an arbitrary 1-D radial conducting model of the mantle first applied to two synthetic models of jerk morphology and then to the 1969 and 2003 jerk morphologies obtained from Le Huy *et al.* (1998) and Olsen & Mandea (2007).

This work demonstrates that: (1) assuming a simultaneous jerk at the CMB, a 1-D mantle conductivity model is able to generate jerk differential time delays at the Earth's surface; (2) synthetic examples of jerk morphology of the X, Y and Z components demonstrated that the pattern of time delays would be different. This would explain why jerks are not seen in observatory data at the same time in different components of the magnetic field and (3) the application of this theory to the 1969 and 2003 jerk morphologies showed that it would also be a natural consequence to have different time delays for each jerk. It is clear that the pattern of time delays at the Earth's surface it is very sensitive to the input model of jerk morphology.

We used two unrealistic mantle conductivity profiles for the Earth, however they illustrated that the observed differential time delays of the order of 2 yr seems to require a highly electrically conducting mantle. The future work involves solving the inverse problem to obtain some constraints on mantle electrical conductivity models based on the observation of differential time delays at the Earth's surface. We can then compare our results with conductivity estimates based on information given by high-pressure experiments simulating the conditions of the deep mantle and with induction studies which mostly estimate the upper-mantle conductivity.

ACKNOWLEDGMENTS

We thank N. Olsen who kindly provided the 2003 geomagnetic jerk model and also A. Kuvshinov and C. Finlay for useful discussions and comments.

REFERENCES

Achache, J., Courtillot, J., Ducruix, J. & Le Mouël, J.-L., 1980. The late 1960's secular variation impulse: further constraints on deep mantle conductivity, *Phys. Earth planet. Inter.*, **23,** 72–75.

Alexandrescu, M., Gilbert, D., Hulot, G., Le Mouël, J.-L. & Saracco, G., 1996. Worldwide wavelet analysis of geomagnetic jerks, *J. geophys. Res.*, **101**(B10), 21 975–21 994,

Alexandrescu, M., Gilbert, D., Le Mouël J-L., Hulot, G. & Saracco, G., 1999. An estimate of average lower mantle conductivity by wavelet analysis of geomagnetic jerks, *J. geophys. Res.*, **104**(B8), 17 735–17 745.

Alldredge, L.R., 1977. Deep mantle conductivity, *J. geophys. Res.*, **82**(33), 5427–5431.

Alldredge, L.R., 1984. A discussion of impulses and jerks in the geomagnetic field, *J. geophys. Res.*, **89,** 4403–4412.

Backus, G.E., 1983. Application of mantle filter theory to the magnetic jerk of 1969, *Geophys. J. R. astr. Soc.*, **74,** 713–746.

Chambodut, A. & Mandea, M., 2005. Evidence for geomagnetic jerks in comprehensive models, *Earth Planets Space*, **57,** 139–149.

Chambodut, A., Eymin, C. & Mandea, M., 2007. Geomagnetic jerks from the earth's surface to the top of the core, *Earth Planets Space*, **59,** 675–684.

Constable, S. & Constable, C., 2004. Observing geomagnetic induction in magnetic satellite measurements and associated implications for mantle conductivity, *Geochem. Geophys. Geosys.* **5,** doi:10.1029/2003GC000634.

De Michelis, P., Cafarella, L. & Meloni, A., 1998. Worldwide character of the 1991 geomagnetic jerk, *Earth planet. Sci. Lett.*, **25**(3), 377–380.

De Michelis, P., Cafarella, L. & Meloni, A., 2000. A global analysis of the 1991 geomagnetic jerk, *Geophys. J. Int.*, **143,** 545–556.

Dobson, D.P. & Brodholt, J.P., 2000. The electrical conductivity of the lower mantle phase magnesiowüstite at high temperatures and pressures, *J. geophys. Res.*, **105**(B1), 531–538.

Gubbins, D. & Roberts, P.H., 1987. Magnetohydrodynamics of the Earth's core in *Geomagnetism*, Chapter 1, Vol. 2, ed. Jacobs, J.A., Academic Press, 1–183.

Gubbins, D. & Tomlinson, L., 1986. Secular variation from monthly means from Apia and Amberley magnetic observatories, *Geophys. J. R. astr. Soc.*, **86,** 603–616.

Iitaka, T., Hirose, K., Kawamura, K. & Murakami, M., 2004. The elasticity of the $MgSiO_3$ post-perovskite phase in the earth's lowermost mantle, *Nature*, **430,** 442–445.

© 2008 The Authors, *GJI*, **173,** 781–792
Journal compilation © 2008 RAS

Kuvshinov, A. & Olsen, N., 2006. A global model of mantle conductivity derived from 5 yr of CHAMP, Ørsted, and SAC-C magnetic data, *Geophys. Res. Lett.*, **33,** L18301, doi:10.1029/2005GL025043.

Lahiri, B.N. & Price, A.T., 1939. Electromagnetic induction in non-uniform conductors, and the determination of the conductivity of the earth from terrestrial magnetic variations, *Phil. Trans. R. Soc. Lond. A.*, **237,** 509–540.

Le Huy, M., Alexandrescu, M., Hulot, G. & Le Mouël, J.-L., 1998. On the characteristics of successive geomagnetic jerks, *Earth Planets Space*, **50,** 723–732.

Macmillan, S., 1996. A geomagnetic jerk for the early 1990's, *Earth plaonet. Sci. Lett.*, **137,** 189–192.

Malin, S.R.C. & Hodder, B.M., 1982. Was the 1970 geomagnetic jerk of internal or external origin? *Nature*, **296,** 726–728.

Mandea, M., Bellanger, E. & Le Mouël. J.-L., 2000. A geomagnetic jerk for the end of the 20th century? *Earth planet. Sci. Lett.*, **183,** 369–373.

Mao, W.L. et al., 2000. Ferromagnesian postperovskite silicates in the D′′ layer of the earth, *PNAS*, **101**(45), 15 867–15 869.

Murakami, M., Hirose, K., Kawamura, K., Sata, N. & Ohishi, Y., 2004. Post-perovskite phase transition in $MgSiO_3$, *Science*, **304,** 855–858.

Nagao, H., Iyemori, T., Higuchi, T., Nakano, S. & Araki, T., 2002. Local time features of geomagnetic jerks, *Earth Planets Space*, **54,** 119–131.

Nagao, H., Iyemori, T., Higuchi, T. & Araki, T., 2003. Lower mantle conductivity anomalies estimated from geomagnetic jerks, *J. geophys. Res.*, **108**(B5), 2254, doi:10.1029/2002JB0011786.

Oganov, A.R. & Ono, S., 2004. Theoretical and experimental evidence for a post-perovskite phase of $MgSiO_3$ in earth's D′′ layer, *Nature*, **430,** 445–448.

Olsen, N., 1999. Long-period (30 days–1 year) electromagnetic sounding and the electrical conductivity of the lower mantle beneath Europe, *Geophys. J. Int.*, **138,** 179–187.

Olsen, N. & Mandea, M., 2007. Investigation of a secular variation impulse using satellite data: the 2003 geomagnetic jerk, *Earth Planets Space*, **255,** 94–105.

Ono, S., Oganov, A.R., Koyama, T. & Shimizu, H., 2006. Stability and compressibility of the high-pressure phases of Al_2O_3 up to 200 GPa: implications for the electrical conductivity of the base of the lower mantle, *Earth planet. Sci. Lett.*, **246,** 326–335.

Runcorn, S.K., 1955. The electrical conductivity of the earth's mantle, *Trans. Am. Geophys. Un.*, **36**(2), 191–198.

Sabaka, T.J., Olsen, N. & Purucker, M.E., 2004. Extending comprehensive models of the earth's magnetic field with Ørsted and CHAMP data, *Geophys. J. Int.,* **159,** 521–547.

Xu, Y., Shankland, T.J. & Poe, B.T., 2000. Laboratory-based electrical conductivity in the earth mantle, *J. geophys. Res.*, **105**(B12), 27 865–27 875.